Supplementary Information

Assessing Melting and Solid-Solid Transition Properties of Choline Chloride via Molecular Dynamics Simulations

Gabriela B. Correa,[†,‡] Dinis O. Abranches,[†,¶] Eliseo Marin-Rimoldi,[†] Yong Zhang,[†] Edward J. Maginn,[*,†] and Frederico W. Tavares[*,‡]

†*Department of Chemical and Biomolecular Engineering, University of Notre Dame, Indiana 46556, USA*

‡*Chemical Engineering Program, Universidade Federal do Rio de Janeiro, Rio de Janeiro 21941-909, Brazil*

¶*CICECO - Aveiro Institute of Materials, Department of Chemistry, University of Aveiro, Aveiro 3810-193, Portugal*

E-mail: ed@nd.edu; tavares@eq.ufrj.br

S.I Methodology

S.I.1 Multistate Bennett Acceptance Ratio Method

The MBAR method[1] is employed for all free energy calculations. In each transformation, a series of K intermediate states is taken into account, each defined by varying conditions such as temperature, volume, or internal energy. The dimensionless free energy of each state k within the transformation are computed numerically using[1,2]

$$f_k = -\ln \sum_{j=1}^{K} \sum_{n=1}^{N_j} \frac{\exp\left[-u_k(\mathbf{r}_{jn})\right]}{\sum_{i=1}^{K} N_i \exp\left[f_i - u_i(\mathbf{r}_{jn})\right]}, \tag{S.1}$$

where N_j represents the number of uncorrelated configurations sampled at state j, and $u_k(\mathbf{r}_{jn})$ denotes the reduced energy of a configuration $\mathbf{r}_{jn}$ sampled at state j relative to state k. Only differences $\Delta f_{i\to k} = f_k - f_i$ are significant; hence, free energies are evaluated as deviations from a particular reference state. The Helmholtz or Gibbs free energy is represented by $F_k = f_k/\beta_k$, given $\beta_k = 1/(k_B T_k)$, where k_B is the Boltzmann constant.

S.I.2 Pseudo-supercritical Path Method

The PSCP method[3–5] predicts melting (T_m) and solid-solid transition (T_{ss}) temperatures by identifying the condition at which the Gibbs free energy difference between the pure phases (liquid, solid, or polymorphs) is zero. It can be modeled across various temperatures as[6,7]

$$\Delta G_{i\to j}(T) = k_{\mathrm{B}} T \left[\Delta f_{i\to j}(T) - \Delta f_{i\to j}(T_{\mathrm{ref}})\right] + \frac{T}{T_{\mathrm{ref}}} \Delta G_{i\to j}(T_{\mathrm{ref}}), \tag{S.2}$$

where i and j represent the pure phases, and T_{ref} is the reference temperature.

The values $\Delta f_{i\to j}$ in Equation (S.2) are obtained from NPT ensemble simulations of each phase over a wide range of temperatures at constant pressure, allowing the construction of relative free energy curves with respect to T_{ref}. During the transformations, the reduced

energy is given by[6,8]

$$u_k(\mathbf{r}) = \beta_k[U(\mathbf{r}) + PV(\mathbf{r})], \tag{S.3}$$

where $U(\mathbf{r})$ denotes the total potential energy, P is the pressure, and V is the system volume.

The value $\Delta G_{i\to j}(T_{\text{ref}})$ in Equation (S.2) is determined by connecting the two phases with PSCP cycles via NVT ensemble simulations at T_{ref}. The PSCP cycles modify the intermolecular potential energy at different steps to obtain information about the Helmholtz free energy, which is then converted into the Gibbs free energy.

In Figure S.1, the PSCP cycle for melting transformations involves a three-step process: downscaling intermolecular interactions of the solid phase (S) to form a dense weak fluid (DWF), expanding the system volume to form a weak fluid (WF) at the liquid density, and restoring intermolecular interactions to form the liquid phase (L). A four-step process occurs for polymorphic transformations in Figure S.2, where polymorph 1 (S1) and polymorph 2 (S2) transition into a dense weak fluid before converging to the same weak fluid state.

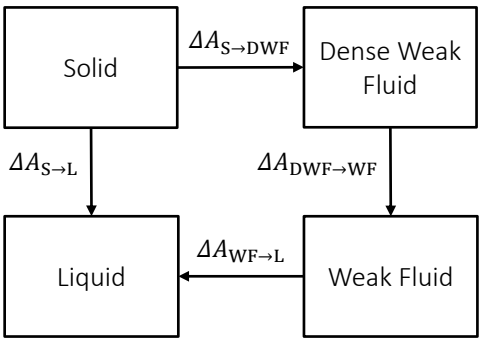

Figure S.1: A schematic of the PSCP cycle for melting transformations.

In the S $\to$ DWF and WF $\to$ L steps, the modification in the intermolecular potential energy is performed via the parameter λ, according to the reduced energy[6,8]

$$u_k(\mathbf{r}) = \beta U(\lambda_k, \mathbf{r}). \tag{S.4}$$

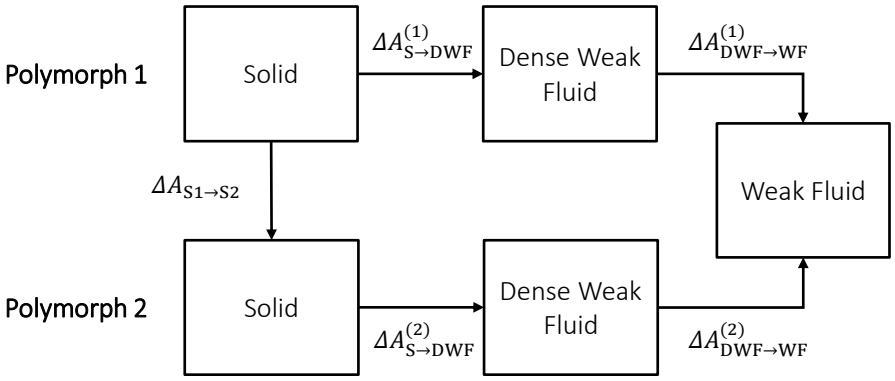

Figure S.2: A schematic of the PSCP cycle for polymorphic transformations.

The magnitude of the interactions is changed for $0 \leq \lambda \leq 1$ as[5]

$$\mathrm{S} \to \mathrm{DWF}: \quad U(\lambda, \mathbf{r}) = S\left(\eta, \tfrac{\lambda}{\lambda_{lj}}\right) U_{lj}(\mathbf{r}) + S\left(\eta^2, \tfrac{\lambda}{\lambda_e}\right) U_e(\mathbf{r}) + \alpha\lambda^2(1-\lambda)^3 U_g(\mathbf{r}), \tag{S.5a}$$

$$\mathrm{WF} \to \mathrm{L}: \quad U(\lambda, \mathbf{r}) = [\eta + \lambda(1-\eta)] U_{lj}(\mathbf{r}) + [\eta + \lambda(1-\eta)]^2 U_e(\mathbf{r}), \tag{S.5b}$$

where $U_{lj}(\mathbf{r})$ and $U_e(\mathbf{r})$ are the Lennard-Jones and electrostatic potentials, respectively, and $U_g(\mathbf{r})$ is the Gaussian tethering potential that restrains atoms close to their equilibrium position in the crystal lattice.

The λ functions in Equation (S.5a) and Equation (S.5b) are used to gradually couple or decouple potentials while maintaining low variance, as shown in our recent work.[5] In the S $\to$ DWF step, we partially decouple Lennard-Jones and electrostatic interactions using the smooth function $S\left(\eta^{m_n}, \frac{\lambda}{\lambda_n}\right)$. Successive coupling and decoupling of the Gaussian potential are achieved using a smooth fifth-order polynomial with parameter $\alpha = 22$. This ensures the reversibility of the cycle by forming a weak solid intermediate state and minimizing ordered-to-disordered phase transition effects. In the WF $\to$ L step, we restore Lennard-Jones and electrostatic interactions using a combination of linear and quadratic functions.

$S\left(\eta^{m_n}, \frac{\lambda}{\lambda_n}\right)$ is a function defined by[5]

$$S(\eta^{m_n}, x) = \begin{cases} (\eta^{m_n} - 1)(3x^2 - 8x + 6)x^2 + 1 & \text{for} \quad 0 \leq x \leq 1 \\ \eta^{m_n} & \text{for} \quad x > 1 \end{cases} . \tag{S.6}$$

This fourth-order polynomial ensures a smooth transition with continuous changes in free energy derivatives. It satisfies $S(\eta^{m_n}, 0) = 1$, $S(\eta^{m_n}, 1) = \eta^{m_n}$, and $S^{(1)}(\eta^{m_n}, 0) = S^{(1)}(\eta^{m_n}, 1) = S^{(2)}(\eta^{m_n}, 1) = 0$, where $S^{(n)}(\eta^{m_n}, x)$ denotes the nth order derivative of $S(\eta^{m_n}, x)$. To achieve low variance, we employ the parameters $\eta = 0.1$, $m_{\text{LJ}} = 1$, $\lambda_{\text{LJ}} = 0.9$, $m_{\text{E}} = 2$, and $\lambda_{\text{E}} = 0.7$.

In the DWF $\rightarrow$ WF step, the expansion of the weakly interacting fluid from a solid-like volume to a liquid-like volume is achieved using the reduced energy[5]

$$u_k(\mathbf{r}) = -N \ln V_k + \beta U(\mathbf{H}_k, \tilde{\mathbf{r}}^{\text{cm}}, \boldsymbol{\delta}), \tag{S.7}$$

where N is the total number of molecules, $\mathbf{H}_k$ is the anisotropic cell matrix of the simulation box, $V_k = \det(\mathbf{H}_k)$ is the box volume, $\tilde{\mathbf{r}}^{\text{cm}}$ represents the reduced coordinates of the centers of mass of molecules, and $\boldsymbol{\delta}$ is the atomic displacements of these centers of mass. The expansion process involves an affine transformation where the scaling of $\mathbf{H}$ and its corresponding volume is done while keeping $\tilde{\mathbf{r}}^{\text{cm}}$ and $\boldsymbol{\delta}$ constants. Therefore, the molecules move far from or closer to each other while preserving their intramolecular configuration and, consequently, improving the overlap between configurations of adjacent intermediate states of the transformation.

The total Helmholtz free energy difference at the selected reference conditions is calculated from the contribution of each step as

$$\Delta A_{\text{S}\rightarrow\text{L}}(T_{\text{ref}}) = \Delta A_{\text{S}\rightarrow\text{DWF}} + \Delta A_{\text{DWF}\rightarrow\text{WF}} + \Delta A_{\text{WF}\rightarrow\text{L}}, \tag{S.8a}$$

$$\Delta A_{\text{s1}\rightarrow\text{s2}}(T_{\text{ref}}) = \Delta A^{(1)}_{\text{S}\rightarrow\text{DWF}} + \Delta A^{(1)}_{\text{DWF}\rightarrow\text{WF}} - \Delta A^{(2)}_{\text{S}\rightarrow\text{DWF}} - \Delta A^{(2)}_{\text{DWF}\rightarrow\text{WF}}. \tag{S.8b}$$

To derive the total Gibbs free energy, we use $\Delta G_{i\rightarrow j}(T_{\text{ref}}) = \Delta A_{i\rightarrow j}(T_{\text{ref}}) + P\Delta V_{i\rightarrow j}(T_{\text{ref}})$.

In practice, the influence of the $P\Delta V_{i\to j}(T_{\mathrm{ref}})$ term on the final transition temperature is minimal, typically less than 0.1 K, thus $\Delta G_{i\to j}(T_{\mathrm{ref}})$ is taken equivalent to $\Delta A_{i\to j}(T_{\mathrm{ref}})$.[9]

Additional properties, such as enthalpy and entropy, can be obtained using the transition temperatures. Enthalpy differences are computed from NPT ensemble simulations at the identified temperatures, taking the ensemble average of enthalpies from each phase as $\Delta H_m = \langle H\rangle_{\mathrm{L}} - \langle H\rangle_{\mathrm{S}}$ and $\Delta H_{ss} = \langle H\rangle_{\mathrm{S2}} - \langle H\rangle_{\mathrm{S1}}$. Consequently, we can obtain entropy differences as $\Delta S_m = \Delta H_m/T_m$ and $\Delta S_{ss} = \Delta H_{ss}/T_{ss}$.

S.I.3 Force Fields

Five force fields were analyzed, as indicated in Table S.1. The GAFF-DES and OPLS-DES force fields were parameterized by Perkins et al.[10] and by Doherty and Acevedo[11], respectively, to describe binary mixtures of ChCl-based DESs. The GAFF-DES force field employed HF/6-31G*-derived charges and a charge scaling factor of 0.9 for ChCl. The OPLS-DES force field employed a charge scaling factor of 0.8, along with adjustments to intermolecular parameters to match site-site radial distribution functions.

Table S.1: Force field parameters studied in this work.

Force Field	Model Description
GAFF-DES	Developed by Perkins et al.[10],[12]
OPLS-DES	Developed by Doherty and Acevedo[11]
GAFF	B3LYP/6-31G charges and LEaP parameters
OPLS	B3LYP/6-31G charges and LigParGen parameters
CHARMM	B3LYP/6-31G charges and CGenFF parameters

The GAFF, OPLS, and CHARMM force fields incorporate Lennard-Jones and intramolecular parameters determined via LEaP,[13] LigParGen,[14] and CGenFF webserver[15] respectively. In addition, partial charges were derived from the B3LYP/6-31G level and the restricted electrostatic potential (RESP) method.[16] In these cases, we used the Gaussian 09 software to optimize the geometry of isolated ions and to calculate the molecular electrostatic potential. We assessed charge scaling factors of 1.0, 0.9, and 0.8 across all investigated force

fields, including GAFF-DES and OPLS-DES, which have predefined values.

S.I.4 Statistical Uncertainty

The determination of the statistical uncertainties for melting and solid-solid transition temperatures involves identifying temperature values where the statistical uncertainty bands intersect the point $\Delta G_{i\to j} = 0$. To assess the uncertainty of the free energy difference, we employ error propagation techniques based on Equation (S.2) as

$$(\delta\beta\Delta G)^2 = (\delta\Delta f)^2 + (\delta\Delta f_{\text{ref}})^2 + (\delta\beta_{\text{ref}}\Delta G_{\text{ref}})^2\,, \tag{S.9}$$

where each term can be directly determined using the MBAR estimator. When calculating the uncertainty of the PSCP cycle, we follow a similar approach to Equation (S.9), propagating errors associated with the contributions at each step of the cycle.

S.I.5 Gaussian Potential

The Gaussian potential is responsible for keeping the atoms in their crystal positions. It is defined as

$$U_g(\mathbf{r}) = -\sum_i \sum_j k_{a,ij} \exp\left(-k_{b,ij} r_{ij}^2\right), \tag{S.10}$$

where k_a is the well depth, k_b is the well width, and $r_{ij} = |\mathbf{r}_i - \mathbf{r}_{\text{well},j}|$ represents the distance between atom i and well j. We use three-dimensional harmonic oscillators to calculate the parameters k_a and k_b, with a probability distribution function

$$P(r) = \left(\frac{\beta\kappa}{\pi}\right)^{3/2} 4\pi r^2 \exp\left(-\beta\kappa r^2\right) dr. \tag{S.11}$$

The well width is set to $k_b = 9\times10^{-2}\text{Å}^2$, while the well depth is determined as $k_a = \kappa/k_b$. The value of κ is derived through curve fitting Equation (S.11) using the probability distribution observed in simulations of crystal phases on the NVT ensemble. This study sampled ions'

center of mass positions to calculate k_a values, which were then used to restrict the positions of heavy atoms, including nitrogen and chlorine.

S.I.6 Simulated Conditions

The systems of forms α and β contained 512 and 500 ion pairs, respectively. Form α had its ion pairs arranged by replicating the unit cell at $8 \times 4 \times 4$, while form β comprised ion pairs replicated in a $5 \times 5 \times 5$ configuration. The temperature range for exploring the melting of form β was 400 K to 1100 K, with increments of 10 K. Solid-solid transitions were investigated within the range of 150 K to 450 K.

PSCP cycle calculations were conducted at reference temperatures specified in Table S.7 and Table S.9. The volumes of the liquid (V_{L}) and solid (V_{S}) phases were determined through NPT simulations at 1 atm. In the S $\rightarrow$ DWF and WF $\rightarrow$ L steps, simulations in the NVT ensemble involved increments of $\Delta\lambda = 0.025$. In the DWF $\rightarrow$ WF step, increments of $\Delta V = (V_{\mathrm{L}} - V_{\mathrm{S}})/20$ were applied.

During the S $\rightarrow$ DWF step, the restraint of nitrogen and chloride atoms was carried out in the crystal structure of form β using Gaussian potential parameters of $k_a = 83.68$ kJ/mol and 41.84 kJ/mol, respectively. For the crystal structure of form α, the restraint of nitrogen, chloride, carbon, and oxygen atoms was performed with $k_a = 41.84$ kJ/mol for all cases.

S.I.7 General Simulation Details

All MD simulations were performed with the LAMMPS package (version 29 September 2021).[17] The simulations were conducted with a time step of 1 fs and under periodic boundary conditions. We constrained the length of every chemical bond involving a hydrogen atom using the SHAKE method.[18] Long-range electrostatic interactions were calculated using the particle-particle-particle-mesh (PPPM) method[19] with a relative error tolerance of 1×10^{-4}.

A cutoff distance of 12 Å was used for Lennard-Jones and electrostatic interactions. For the CHARMM force field, Lennard-Jones interactions were smoothly switched between

11 Å and 12 Å. Tail corrections were used for the other force fields to account for long-range dispersion interactions.

Temperature control was executed by the Nosé-Hoover chain[20] with three thermostats and a characteristic time of 100 fs. Pressure control was executed by the Martyna-Tobias-Klein barostat[21] with a characteristic time of 1000 fs. In constant-pressure simulations, the pressure was set at 1 atm, considering isotropic volume fluctuations in the liquid phase and anisotropic cell fluctuations in the solid phase. Each PSCP step consisted of 5 ns, with samples collected every 200 fs during the final 3 ns.

Input files and initial configurations were generated with the Playmol package.[22] The liquid configurations were obtained by random packing. The crystal configurations were obtained by replicating experimental unit cells taken from the Cambridge Structural Database (CSD).[23] The ChCl polymorphs and their CSD identifications are: form α ID 1937745[24] and form β ID 1124454.[25]

Free energy values for the PSCP method were evaluated using the MBAR method from the PYMBAR library (version 3.0.5).[1] Uncertainties were calculated using the MBAR estimator,[1,2] with propagation managed by the delta method, and results reported in 95% confidence intervals. The decorrelation of the dataset was performed using the autocorrelation function and correlation time based on the total potential energy data.

Additional details can be found in Section S.I of the Supplementary Material regarding the formulation of the MBAR method, the functions governing intermolecular interactions during the PSCP cycle, and error propagation calculations. We also provide information about the simulated values of temperature, volume, and λ, alongside the parameters of the Gaussian tethering potential and the number of ion pairs in the systems.

A repository containing the Python and LAMMPS scripts we used is available at `github.com/atoms-ufrj/CHCL-article-2024`. It also includes a customized version of the LAMMPS `dihedral_style charmm` command, which was applied to couple and decouple Lennard-Jones interactions within the CHARMM force field.

S.II Atomic Positions of Form β Unit Cell

```
88
choline chloride form beta unit cell - xyz file
Cl1         0.00000         0.00000         9.41400
Cl1         0.00000         4.70700         4.70700
Cl1         4.70700         0.00000         4.70700
Cl1         4.70700         4.70700         9.41400
N1          4.70700         4.70700         4.70700
C4          5.62000         5.73000         5.39400
C5          4.89400         6.91000         6.05400
O1          5.84900         7.83600         6.57200
H1          5.66600         7.91800         7.52900
C1          3.72500         5.35300         3.74800
C2          3.94300         3.90800         5.74700
C3          5.57500         3.71600         3.93200
H4A         6.30700         6.11200         4.62800
H4B         6.23300         5.19200         6.12800
H5A         4.29500         7.46400         5.32600
H5B         4.23300         6.58800         6.86100
H1A         4.29200         5.97400         3.04700
H1B         3.02100         5.96400         4.31500
H1C         3.19100         4.56600         3.20700
H2A         3.36200         3.15400         5.21300
H2B         3.29200         4.59000         6.29700
H2C         4.66200         3.42400         6.41200
H3A         6.15200         4.27600         3.19000
H3B         4.92200         2.99900         3.42800
```

H3C	6.24600	3.21400	4.63500
N1	4.70700	0.00000	9.41400
C4	5.53400	0.93400	10.30400
C5	4.73200	1.65900	11.39400
O1	5.49300	2.73500	11.93300
H1	0.06100	8.67800	11.61200
C1	3.84200	0.82800	8.45500
C2	3.79600	-0.91500	10.21400
C3	5.64600	-0.83900	8.55700
H4A	6.05300	1.64100	9.64600
H4B	6.30800	0.32100	10.78300
H5A	3.78000	2.05900	11.03600
H5B	4.51000	0.97300	12.21800
H1A	4.50200	1.46500	7.86200
H1B	3.14600	1.43300	9.03700
H1C	3.29000	0.13800	7.81200
H2A	3.29500	-1.60000	9.52400
H2B	3.05900	-0.30900	10.74600
H2C	4.41400	-1.47400	10.92300
H3A	6.28100	-0.16800	7.97200
H3B	5.04700	-1.48000	7.90300
H3C	6.25700	-1.45400	9.22400
N1	0.00000	4.70700	9.41400
C4	0.73900	5.85000	10.14200
C5	-0.15300	7.00400	10.61200
O1	0.64400	7.95800	11.30800
H1	5.39300	3.48600	11.29200

C1	-0.56800	5.16700	8.09900
C2	-1.07800	4.07100	10.27000
C3	1.06800	3.64900	9.19200
H4A	1.51400	6.22800	9.46300
H4B	1.25000	5.41400	11.01100
H5A	-0.62700	7.51100	9.76800
H5B	-0.92300	6.65500	11.30400
H1A	0.23300	5.64600	7.53600
H1B	-1.36800	5.88600	8.29900
H1C	-0.98500	4.29700	7.58800
H2A	-1.49600	3.21500	9.73200
H2B	-1.86500	4.80800	10.44700
H2C	-0.63200	3.75300	11.21700
H3A	1.82800	4.06500	8.53200
H3B	0.57500	2.78800	8.76800
H3C	1.50500	3.37100	10.15700
N1	0.00000	0.00000	4.70700
C4	1.04900	0.88200	5.35100
C5	0.46000	1.85600	6.33400
O1	1.37600	2.91400	6.54600
H1	1.04900	3.62400	5.92900
C1	-0.86900	0.79500	3.74900
C2	-0.84800	-0.72500	5.74000
C3	0.78800	-1.04500	3.90800
H4A	1.59000	1.39900	4.55100
H4B	1.75500	0.23200	5.87800
H5A	-0.51700	2.25100	6.04900

H5B	0.30600	1.36300	7.27200
H1A	-0.22200	1.36200	3.07300
H1B	-1.52400	1.45800	4.31600
H1C	-1.47700	0.08700	3.17600
H2A	-1.49000	-1.43600	5.21100
H2B	-1.47000	0.00200	6.26700
H2C	-0.18200	-1.26000	6.42200
H3A	1.40700	-0.52600	3.16900
H3B	0.07500	-1.70600	3.40600
H3C	1.40900	-1.62100	4.60100

S.III Lattice Parameters and Solid Density

Table S.2: Summary of average lattice parameters and densities for choline chloride form α at 295 K.

	a (Å)	b (Å)	c (Å)	α (°)	β (°)	γ (°)	ρ (g/cm^3)
Ref. 26	5.901	11.589	11.210	90.0	90.0	90.0	1.210
			Charge Scaling 1.0				
GAFF-DES	5.903	11.404	11.812	90.0	90.0	90.0	1.166
OPLS-DES	6.671	10.915	11.212	90.1	90.1	89.6	1.136
GAFF	5.937	11.383	11.763	90.0	90.0	90.0	1.167
OPLS	6.966	11.069	10.436	90.0	90.0	90.0	1.153
CHARMM	6.185	10.731	12.182	90.0	90.0	90.0	1.151
			Charge Scaling 0.9				
GAFF-DES	5.954	11.532	11.928	90.0	90.0	90.0	1.132
OPLS-DES	6.849	10.888	11.210	90.6	89.6	89.7	1.110
GAFF	5.990	11.507	11.882	90.0	90.0	90.0	1.132
OPLS	7.047	11.033	10.563	90.0	89.9	90.0	1.129
CHARMM	6.083	11.361	11.672	90.0	90.0	90.0	1.150
			Charge Scaling 0.8				
GAFF-DES	6.011	11.685	12.069	90.0	90.0	90.0	1.094
OPLS-DES	6.791	10.859	11.406	89.8	90.3	90.0	1.103
GAFF	6.053	11.661	12.022	90.0	90.0	90.0	1.093
OPLS	6.684	11.211	11.621	89.2	90.6	90.0	1.065
CHARMM	6.619	11.689	11.449	88.1	89.9	88.3	1.049

Table S.3: Summary of average lattice parameters and densities for choline chloride form β at 358 K.

	a (Å)	b (Å)	c (Å)	α (°)	β (°)	γ (°)	ρ (g/cm^3)
Ref. 25	9.414	9.414	9.414	90.0	90.0	90.0	1.111
				Charge Scaling 1.0			
GAFF-DES	9.551	9.589	9.622	89.9	90.0	90.0	1.052
OPLS-DES	9.406	9.339	9.272	90.1	90.0	90.1	1.139
GAFF	9.614	9.576	9.611	90.1	90.0	90.1	1.048
OPLS	9.501	9.551	9.441	90.0	89.9	89.8	1.083
CHARMM	9.346	9.598	9.631	90.0	90.0	90.1	1.074
				Charge Scaling 0.9			
GAFF-DES	9.693	9.722	9.683	90.0	90.0	90.0	1.017
OPLS-DES	9.020	9.764	9.504	90.2	90.0	90.1	1.108
GAFF	9.683	9.750	9.692	90.0	90.0	90.0	1.014
OPLS	9.463	9.573	9.709	90.0	90.0	90.0	1.054
CHARMM	9.672	9.578	9.623	90.0	90.0	90.0	1.040
				Charge Scaling 0.8			
GAFF-DES	9.823	9.820	9.815	90.0	90.0	90.0	0.980
OPLS-DES	9.529	9.447	9.625	89.9	89.9	89.9	1.070
GAFF	9.838	9.819	9.815	90.0	90.0	90.0	0.978
OPLS	9.676	9.713	9.644	90.0	90.0	90.0	1.023
CHARMM	9.744	9.753	9.747	90.0	90.0	90.0	1.001

Table S.4: Relative deviation of average lattice parameters and densities for forms α and β.

	Charge	form α				form β			
	Scaling	d_ρ (%)	d_a (%)	d_b (%)	d_c (%)	d_ρ (%)	d_a (%)	d_b (%)	d_c (%)
	1.0	−3.6	+0.0	−1.6	+5.4	−5.3	+1.4	+1.9	+2.2
GAFF-DES	0.9	−6.5	+0.9	−0.5	+6.4	−8.5	+3.0	+3.3	+2.9
	0.8	−9.6	+1.9	+0.8	+7.7	−11.9	+4.3	+4.3	+4.3
	1.0	−6.1	+13.0	−5.8	+0.0	+2.5	−0.1	−0.8	−1.5
OPLS-DES	0.9	−8.2	+16.1	−6.1	+0.0	−0.3	−4.2	+3.7	+1.0
	0.8	−8.8	+15.1	−6.3	+1.7	−3.7	+1.2	+0.4	+2.2
	1.0	−3.6	+0.6	−1.8	+4.9	−5.7	+2.1	+1.7	+2.1
GAFF	0.9	−6.5	+1.5	−0.7	+6.0	−8.7	+2.9	+3.6	+3.0
	0.8	−9.7	+2.6	+0.6	+7.2	−12.0	+4.5	+4.3	+4.3
	1.0	−4.7	+18.0	−4.5	−6.9	−2.5	+0.9	+1.5	+0.3
OPLS	0.9	−6.7	+19.4	−4.8	−5.8	−5.1	+0.5	+1.7	+3.1
	0.8	−12.0	+13.3	−3.3	+3.7	−7.9	+2.8	+3.2	+2.4
	1.0	−4.9	+4.8	−7.4	+8.7	−3.3	−0.7	+2.0	+2.3
CHARMM	0.9	−5.0	+3.1	−2.0	+4.1	−5.9	+2.7	+1.7	+2.2
	0.8	−13.3	+12.2	+0.9	+2.1	−9.9	+3.5	+3.6	+3.5

S.IV Initial Phase Transition Analysis

The solid-solid and solid-liquid transitions were first studied by analyzing how the polymorph structures change at different temperatures. Density profiles were collected for each polymorph in a temperature range of 150 K to 1100 K using NPT ensemble simulations over 40 ns. The data are presented in Figure S.3 for all force fields and charge scaling factors.

In all cases, two transitions were observed when simulating form α, characterized by sharp changes in the system density. The first transition happens around 320−450 K for the GAFF-DES, GAFF, and CHARMM force fields, and around 210−270 K for the OPLS-DES and OPLS force fields. This transition signifies a change from form α to a new crystal form, as detailed in the following paragraphs. The second transition, occurring around 500−920 K, involves the melting of the new structure. Form β showed no transitions between different solid phases, only melting at temperatures around 600−1070 K. In general, the higher the charge scaling factor, the higher the transition temperatures.

The form α structures were evaluated before and after the solid-solid transition using radial pair distribution function, as illustrated in Figure S.4 for the OPLS-DES force field at a charge scaling factor of 0.9. Prior to the transition at 200 K, the results indicate a strong periodicity in solid structure interactions. Following the transition at 400 K, the nitrogen and chloride atoms regularity is maintained, while the carbon and oxygen atoms mobility increases. Consequently, form α can be classified as a disordered crystal after the transition, resembling form β.

The disordered form α does not precisely match form β, as it presents distinct properties, such as lattice parameters, densities, and melting temperatures. Therefore, we observe the emergence of a disordered metastable phase α, solely observable in simulations and not reported experimentally. In an ideal situation, the disordered form α should be equivalent to form β. However, it does not occur due to difficulties in transitioning between two solid phases via direct heating in molecular simulation, constrained by time scale limitations and energy barriers.

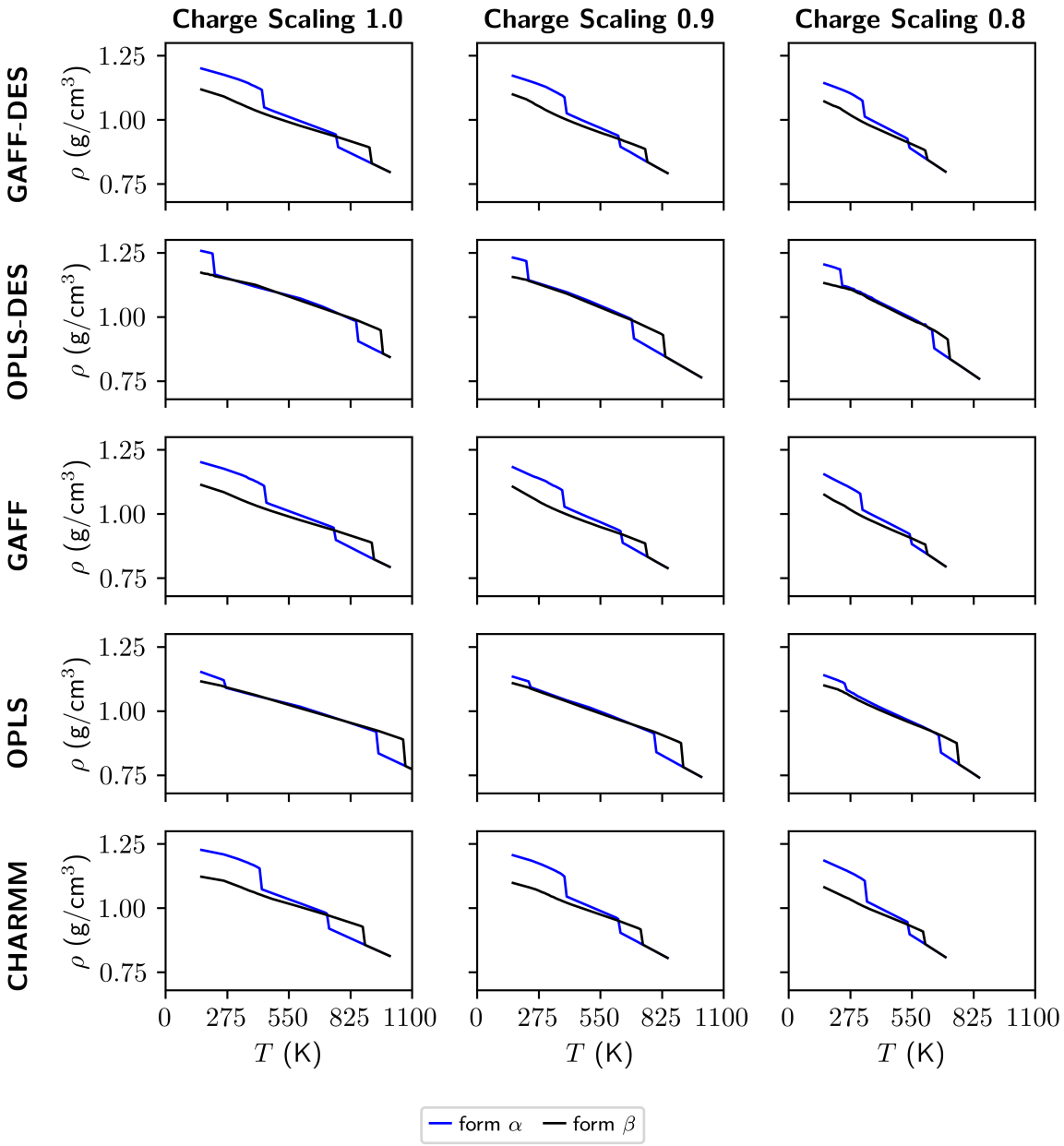

Figure S.3: Behavior of solid density in forms α and β for different temperatures considering different force fields and charge scaling factors.

We determined the initial estimates of the solid-solid transition temperatures as the point where form α changes to the new disordered crystal. The initial estimates of the melting temperatures were taken as the point where form β transitions to the liquid phase. The values are provided in Table S.5. It is important to note that these data overestimate the transition temperatures due to superheating effects. However, they are important for establishing the

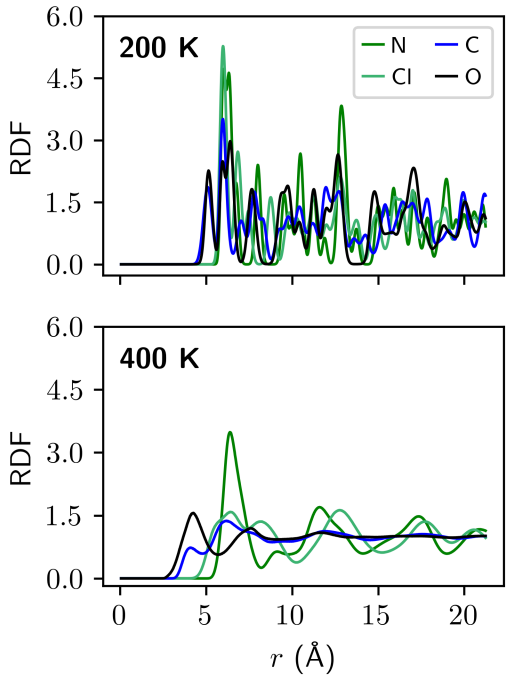

Figure S.4: Intermolecular radial pair distribution function of form α for oxygen, carbon, nitrogen, and chloride atoms at 200 K and 400 K, considering the OPLS-DES force field at a charge scaling factor of 0.9.

conditions of the PSCP simulations, ensuring that T_{ref} was set below the initial estimates, beyond which no further structures of interest are observed.

Table S.5: Initial estimates of the solid-solid transition and melting temperatures.

	Charge Scaling	T_{ss} (K)	T_m (K)
GAFF-DES	1.0	430−440	910−920
	0.9	390−400	750−760
	0.8	330−340	610−620
OPLS-DES	1.0	210−220	960−970
	0.9	220−230	830−840
	0.8	230−240	710−720
GAFF	1.0	440−450	920−930
	0.9	380−390	750−760
	0.8	320−330	610−620
OPLS	1.0	260−270	1060−1070
	0.9	230−240	910−920
	0.8	250−260	750−760
CHARMM	1.0	420−430	880−890
	0.9	390−400	730−740
	0.8	340−350	600−610

S.V Solid-Solid Transition Properties

Table S.6: Solid-solid transition properties of choline chloride calculated using the PSCP method. Value found in the literature is also provided. Numbers within parentheses indicate the statistical uncertainty in the last digit.

	Charge Scaling	T_{ss} (K)	ΔH_{ss} (kJ/mol)	ΔS_{ss} (J/mol/K)
Ref. 27	–	352.3(1)	16.4(7)	47(2)
GAFF-DES	1.0	348(5)	17.4(4)	50(1)
	0.9	303(6)	15.6(4)	52(2)
	0.8	268(4)	14.3(4)	53(2)
OPLS-DES	1.0	–	–	–
	0.9	–	–	–
	0.8	–	–	–
GAFF	1.0	358(4)	20.3(5)	57(2)
	0.9	320(4)	17.7(3)	56(1)
	0.8	281(4)	15.9(3)	57(1)
OPLS	1.0	–	–	–
	0.9	–	–	–
	0.8	213(8)	3.7(9)	17(4)
CHARMM	1.0	408(6)	16.1(4)	40(1)
	0.9	347(5)	15.2(4)	44(1)
	0.8	314(5)	14.2(3)	45(1)

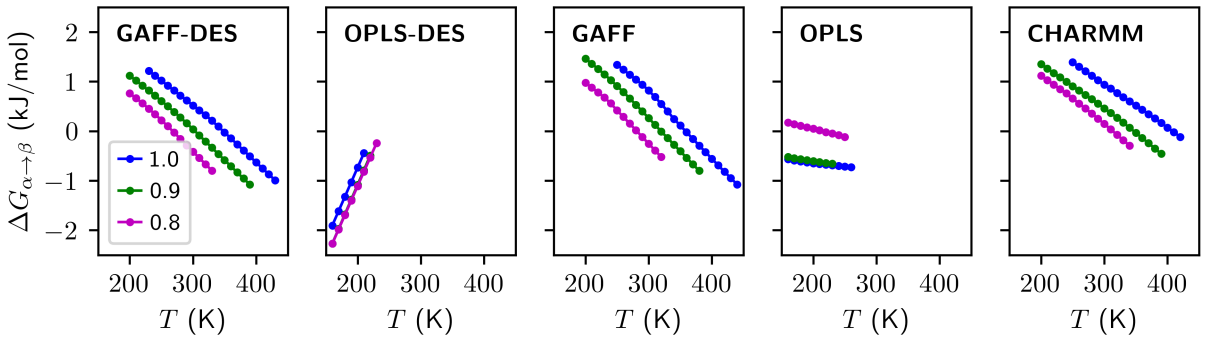

Figure S.5: Free energy difference between forms α and β for different temperatures considering different force fields and charge scaling factors.

Table S.7: Free energy contributions of the PSCP method for the solid-solid transition of choline chloride. Numbers within parentheses indicate the statistical uncertainty in the last digit.

	Charge Scaling	T_{ref} (K)	$\Delta A^{(1)}_{\mathrm{S}\to\mathrm{DWF}}$ (kJ/mol)	$\Delta A^{(1)}_{\mathrm{DWF}\to\mathrm{WF}}$ (kJ/mol)	$\Delta A^{(2)}_{\mathrm{S}\to\mathrm{DWF}}$ (kJ/mol)	$\Delta A^{(2)}_{\mathrm{DWF}\to\mathrm{WF}}$ (kJ/mol)
GAFF-DES	1.0	360	387.47(7)	−4.759(1)	382.15(2)	1.174(1)
	0.9	360	304.37(7)	−4.018(1)	302.11(4)	1.209(1)
	0.8	300	243.62(2)	−2.981(1)	241.00(7)	1.370(1)
OPLS-DES	1.0	200	542.68(9)	−10.448(1)	540.55(9)	−5.242(1)
	0.9	200	435.08(9)	−8.863(1)	435.40(9)	−4.641(1)
	0.8	200	340.15(9)	−6.762(1)	340.52(9)	−2.486(1)
GAFF	1.0	360	560.90(6)	−4.805(1)	554.84(4)	1.349(1)
	0.9	360	444.79(7)	−4.029(1)	441.87(6)	1.174(1)
	0.8	300	354.42(2)	−3.004(1)	351.14(7)	1.334(1)
OPLS	1.0	200	294.30(9)	−3.263(1)	297.37(9)	−3.623(1)
	0.9	200	231.50(9)	−2.058(1)	234.64(9)	−2.657(1)
	0.8	200	181.29(9)	−2.428(1)	179.81(9)	−1.147(1)
CHARMM	1.0	360	724.77(6)	−7.603(1)	715.66(2)	−0.307(1)
	0.9	360	578.48(2)	−6.346(1)	572.47(2)	0.241(1)
	0.8	300	460.12(7)	−4.995(1)	453.99(5)	0.523(1)

S.VI Disordered Nature of Form β

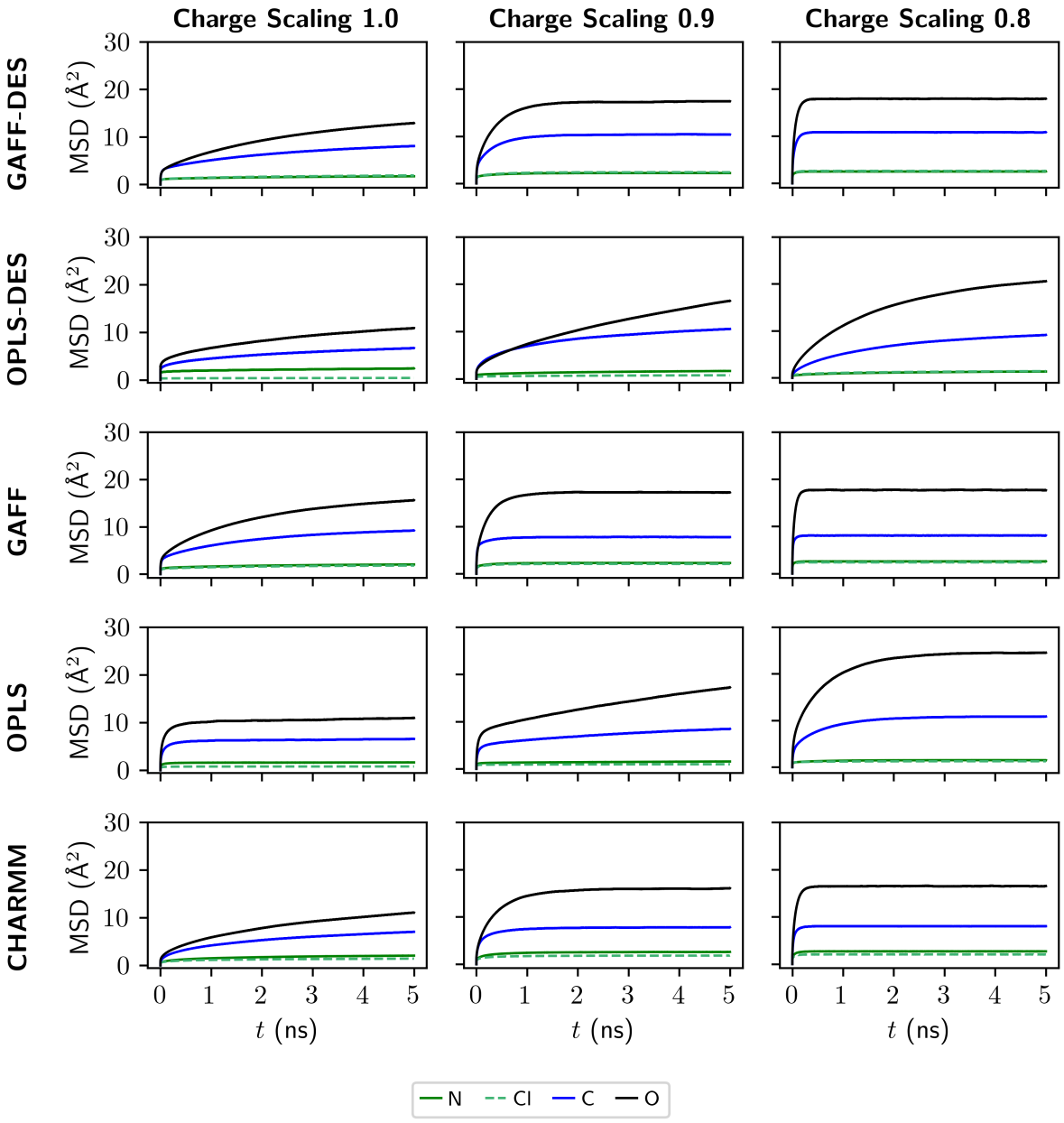

Figure S.6: Mean squared displacement of form β for oxygen, carbon, nitrogen, and chloride atoms at 358 K considering different force fields and charge scaling factors. Data for the nitrogen and chloride atoms are almost identical.

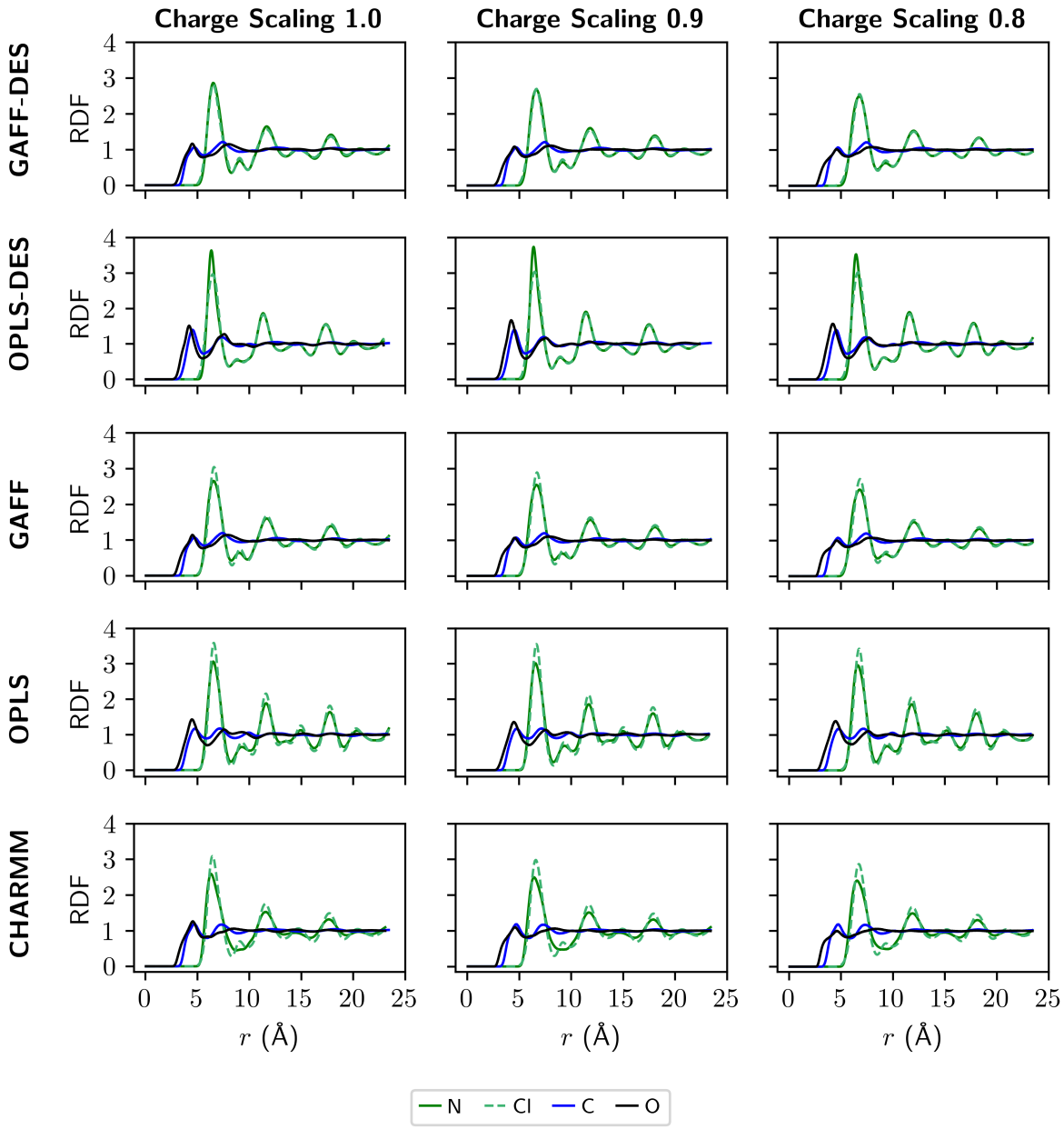

Figure S.7: Intermolecular radial pair distribution function of form β for oxygen, carbon, nitrogen, and chloride atoms at 358 K considering different force fields and charge scaling factors. Data for the nitrogen and chloride atoms are almost identical.

S.VII Melting Properties

Table S.8: Melting properties of choline chloride form β calculated using the PSCP method. Values found in the literature are also provided. Numbers within parentheses indicate the statistical uncertainty in the last digit.

	Charge Scaling	T_m (K)	ΔH_m (kJ/mol)	ΔS_m (J/mol/K)
Ref. 28	–	597(7)	4.3(6)	7.2(9)
Ref. 29	–	597(7)	7.7(1)	12.9(4)
Ref. 30	–	687(9)	13.8(3)	20.1(5)
GAFF-DES	1.0	759(4)	11.0(5)	14.5(7)
	0.9	619(4)	7.7(5)	12.4(8)
	0.8	473(6)	4.2(5)	9(1)
OPLS-DES	1.0	860(3)	17.9(2)	20.8(2)
	0.9	745(3)	15.3(2)	20.5(3)
	0.8	636(3)	12.3(2)	19.3(3)
GAFF	1.0	748(4)	10.9(4)	14.6(5)
	0.9	617(4)	7.8(4)	12.6(7)
	0.8	478(7)	4.3(4)	9.0(8)
OPLS	1.0	920(3)	19.8(3)	21.5(3)
	0.9	787(3)	16.2(3)	20.6(4)
	0.8	651(3)	12.6(2)	19.2(3)
CHARMM	1.0	759(6)	10.2(5)	13.4(7)
	0.9	627(6)	7.8(7)	12.4(9)
	0.8	509(8)	5.5(6)	11(1)

Table S.9: Free energy contributions of the PSCP method for the melting of choline chloride form β. Numbers within parentheses indicate the statistical uncertainty in the last digit.

	Charge Scaling	T_{ref} (K)	$\Delta A_{\mathrm{S}\to\mathrm{DWF}}$ (kJ/mol)	$\Delta A_{\mathrm{DWF}\to\mathrm{WF}}$ (kJ/mol)	$\Delta A_{\mathrm{WF}\to\mathrm{L}}$ (kJ/mol)
GAFF-DES	1.0	730	330.95(5)	−2.704(1)	−327.84(2)
	0.9	640	264.94(5)	−2.003(1)	−263.21(2)
	0.8	440	221.82(9)	0.163(1)	−221.72(2)
OPLS-DES	1.0	840	439.82(5)	−7.987(1)	−431.41(2)
	0.9	720	354.23(6)	−6.364(1)	−347.36(2)
	0.8	660	271.90(9)	−5.578(1)	−266.79(2)
GAFF	1.0	730	504.13(6)	−2.875(1)	−501.01(2)
	0.9	640	405.16(7)	−1.758(1)	−403.71(2)
	0.8	440	332.43(6)	0.076(1)	−332.21(2)
OPLS	1.0	840	193.95(5)	−6.894(1)	−185.28(2)
	0.9	720	152.21(5)	−5.343(1)	−145.57(2)
	0.8	660	109.72(2)	−4.901(1)	−105.00(2)
CHARMM	1.0	730	667.38(6)	−3.991(1)	−663.02(2)
	0.9	600	541.55(7)	−2.509(1)	−538.72(2)
	0.8	440	435.59(4)	−0.723(1)	−434.21(2)

References

(1) Shirts, M. R.; Chodera, J. D. Statistically optimal analysis of samples from multiple equilibrium states. *J. Chem. Phys.* **2008**, *129*, 124105, DOI: 10.1063/1.2978177.

(2) Kong, A.; McCullagh, P.; Meng, X.; Nicolae, D.; Tan, Z. A theory of statistical models for Monte Carlo integration. *J. R. Stat. Soc., Ser. B: Stat. Methodol.* **2003**, *65*, 585–604, DOI: 10.1111/1467-9868.00404.

(3) Eike, D. M.; Brennecke, J. F.; Maginn, E. J. Toward a robust and general molecular simulation method for computing solid-liquid coexistence. *J. Chem. Phys.* **2005**, *122*, 014115, DOI: 10.1063/1.1823371.

(4) Eike, D. M.; Maginn, E. J. Atomistic simulation of solid-liquid coexistence for molecular systems: Application to triazole and benzene. *J. Chem. Phys.* **2006**, *124*, 164503, DOI: 10.1063/1.2188400.

(5) Correa, G. B.; Zhang, Y.; Abreu, C. R. A.; Tavares, F. W.; Maginn, E. J. Revisiting the pseudo-supercritical path method: An improved formulation for the alchemical calculation of solid-liquid coexistence. *J. Chem. Phys.* **2023**, *159*, 104105, DOI: 10.1063/5.0163564.

(6) Schieber, N. P.; Dybeck, E. C.; Shirts, M. R. Using reweighting and free energy surface interpolation to predict solid-solid phase diagrams. *J. Chem. Phys.* **2018**, *148*, 144104, DOI: 10.1063/1.5013273.

(7) Yang, M.; Dybeck, E.; Sun, G.; Peng, C.; others Prediction of the relative free energies of drug polymorphs above 0 K. *Cryst. Growth Des.* **2020**, *20*, 5211–5224, DOI: 10.1021/acs.cgd.0c00422.

(8) Bauer, G.; Gross, J. Phase Equilibria of Solid and Fluid Phases from Molecular Dynam-

ics Simulations with Equilibrium and Nonequilibrium Free Energy Methods. *J. Chem. Theory Comput.* **2019**, *15*, 3778–3792, DOI: 10.1021/acs.jctc.8b01023.

(9) DeFever, R. S.; Wang, H.; Zhang, Y.; Maginn, E. J. Melting points of alkali chlorides evaluated for a polarizable and non-polarizable model. *J. Chem. Phys.* **2020**, *153*, 011101, DOI: 10.1063/5.0012253.

(10) Perkins, S. L.; Painter, P.; Colina, C. M. Experimental and Computational Studies of Choline Chloride-Based Deep Eutectic Solvents. *J. Chem. Eng. Data* **2014**, *59*, 3652–3662, DOI: 10.1021/je500520h.

(11) Doherty, B.; Acevedo, O. OPLS Force Field for Choline Chloride-Based Deep Eutectic Solvents. *J. Phys. Chem. B* **2018**, *122*, 9982–9993, DOI: 10.1021/acs.jpcb.8b06647.

(12) Perkins, S. L.; Painter, P.; Colina, C. M. Molecular Dynamic Simulations and Vibrational Analysis of an Ionic Liquid Analogue. *J. Phys. Chem. B* **2013**, *117*, 10250–10260, DOI: 10.1021/jp404619x.

(13) Case, D.; others Amber 2021. *University of California, San Francisco* **2021**,

(14) Dodda, L. S.; Vilseck, J. Z.; Tirado-Rives, J.; Jorgensen, W. L. 1.14*CM1A-LBCC: Localized Bond-Charge Corrected CM1A Charges for Condensed-Phase Simulations. *J. Phys. Chem. B* **2017**, *121*, 3864–3870, DOI: 10.1021/acs.jpcb.7b00272.

(15) Vanommeslaeghe, K.; others CHARMM General Force Field (CGenFF): A force field for drug-like molecules compatible with the CHARMM all-atom additive biological force fields. *J. Comput. Chem.* **2010**, *31*, 671–690, DOI: 10.1002/jcc.21367.

(16) Bayly, C. I.; Cieplak, P.; Cornell, W. D.; Kollman, P. A. A well-behaved electrostatic potential based method using charge restraints for deriving atomic charges: The RESP model. *J. Chem. Phys.* **1993**, *97*, 10269–10280, DOI: 10.1021/j100142a004.

(17) Thompson, A. P.; Aktulga, H. M.; Berger, R.; Bolintineanu, D. S.; Brown, W. M.; Crozier, P. S.; in 't Veld, P. J.; Kohlmeyer, A.; Moore, S. G.; Nguyen, T. D.; Shan, R.; Stevens, M. J.; Tranchida, J.; Trott, C.; Plimpton, S. J. LAMMPS - A flexible simulation tool for particle-based materials modeling at the atomic, meso, and continuum scales. *Comput. Phys. Commun.* **2022**, *271*, 108171, DOI: 10.1016/j.cpc.2021.108171.

(18) Ryckaert, J.-P.; Ciccotti, G.; Berendsen, H. J. C. Numerical integration of the cartesian equations of motion of a system with constraints: molecular dynamics of n-alkanes. *J. Comp. Phys.* **1977**, *23*, 327–341, DOI: 10.1016/0021-9991(77)90098-5.

(19) Toukmaji, A. Y.; Board, Jr., J. A. Ewald summation techniques in perspective: A survey. *Comput. Phys. Commun.* **1996**, *95*, 73–92, DOI: 10.1016/0010-4655(96)00016-1.

(20) Martyna, G. J.; Klein, M. L.; Tuckerman, M. E. Nosé-Hoover chains: The canonical ensemble via continuous dynamics. *J. Chem. Phys.* **1992**, *97*, 2635–2643, DOI: 10.1063/1.463940.

(21) Martyna, G. J.; Tobias, D. J.; Klein, M. L. Constant pressure molecular dynamics algorithms. *J. Chem. Phys.* **1994**, *101*, 4177–4189, DOI: 10.1063/1.467468.

(22) Abreu, C. R. A. Playmol. **2021**, DOI: https://github.com/atoms{ufrj/playmol.

(23) Groom, C. R.; Bruno, I. J.; Lightfoot, M. P.; Ward, S. C. The Cambridge Structural Database. *Acta Cryst.* **2016**, *B72*, 171–179, DOI: 10.1107/S2052520616003954.

(24) Edgehouse, K.; Chen, B.; Gurkan, B.; Pentzer, E. CCDC 1937745. *CSD Communication* **2019**, DOI: 10.5517/ccdc.csd.cc231cxg.

(25) Petrouleas, V.; others Xray diffraction study of choline chloride's β form. *J. Chem. Phys.* **1978**, *68*, 2243–2248, DOI: 10.1063/1.435993.

(26) Hjortås, J.; Sørum, H. A re-investigation of the crystal structure of choline chloride. *Acta Cryst. B* **1971**, *27*, 1320–1323, DOI: 10.1107/S0567740871003935.

(27) Alhadid, A.; Jandl, C.; Mokrushina, L.; Minceva, M. Cocrystal Formation in Choline Chloride Deep Eutectic Solvents. *Cryst. Growth Des.* **2022**, *22*, 1933–1942, DOI: 10.1021/acs.cgd.1c01477.

(28) Fernandez, L.; Silva, L. P.; Martins, M. A. R.; Ferreira, O.; Ortega, J.; Pinho, S. P.; Coutinho, J. A. P. Indirect assessment of the fusion properties of choline chloride from solid-liquid equilibria data. *Fluid Phase Equilibria* **2017**, *448*, 9–14, DOI: 10.1016/j.fluid.2017.03.015.

(29) Vilas-Boas, S. M.; Abranches, D. O.; Crespo, E. A.; Ferreira, O.; Coutinho, J. A.; Pinho, S. P. Experimental solubility and density studies on aqueous solutions of quaternary ammonium halides, and thermodynamic modelling for melting enthalpy estimations. *Journal of Molecular Liquids* **2020**, *300*, 112281, DOI: 10.1016/j.molliq.2019.112281.

(30) van den Bruinhorst, A.; Avila, J.; Rosenthal, M.; Pellegrino, A.; Burghammer, M.; Gomes, M. C. Defying decomposition: the curious case of choline chloride. *Nature Communications* **2023**, *14*, 6684, DOI: 10.1038/s41467-023-42267-6.